Reports

Momentum Transport in Turbulent Flow between Concentric Rotating Cylinders

Abstract. *Apparent shear stress in turbulent flow between a stationary inner cylinder and a rotating outer cylinder is measured by computing radial flux of tangential momentum by use of velocities obtained from photographs of successive positions of marker particles assumed to represent the fluid motion. Values are consistent with total shear stress at the inner cylinder found by measuring the velocity gradient.*

Bagnold (*1*), experimenting on flows of water containing neutrally buoyant solid particles between a stationary inner cylinder and a coaxial rotating outer cylinder, observed an excess normal stress on the inner cylinder. He assumed that this was caused by collisions of the particles with the boundary, and on this basis developed a theory (*2*) that shearing of a fluid containing sediment grains causes the grains to come into contact, and that in open-channel flow the dispersive forces generated by these collisions cause grains to be supported independently of the fluid turbulence.

Rather than reflecting grain collisions throughout the flow, Bagnold's excess normal stress may be an inner-boundary effect peculiar to the flow system. The general importance of grain collisions in turbulent shear flows with appreciable sediment concentrations has yet to be demonstrated. The lack of a firm test of the theory prompted me to study a similar flow system from a different standpoint, by following motions of fluid and grains in the flow. If the neutrally buoyant grains move passively with the fluid, their contribution to radial flux of forward momentum is nearly the same as an equivalent volume of fluid, so that the ratio of rates of momentum transport due to grain motions and to fluid motions (the momentum transport ratio) would equal the ratio of volume of grains to volume of fluid in the flow, but if grain collisions are important, the momentum transport ratio should be significantly larger, reflecting disproportionate momentum transport by the colliding grains. This report describes preliminary experiments showing that the basis of the method, evaluation of momentum flux by photographing trajectories of small marker particles, gives the expected magnitudes.

The apparatus (Fig. 1) consists of concentric lucite cylinders terminated by lucite disks. The inner cylinder is supported only by bearings above and below, and was held fixed while the outer cylinder and end plates were rotated. Theoretically the flow, though turbulent when first set in motion, should be laminar at any rotation rate after an initial transient stage (*3, 4*). Continuing turbulence in real rotating-cylinder flow is caused by minor irregularities in equipment (*4*). The outer cylinder was rotated at 136 rev/min, in the range for continuing existence of turbulence (*5*), although strong turbulence is restricted to the inner part of the annulus owing to inherent flow stability and the tendency for shear to be concentrated near the inner boundary by rotation of the end plates.

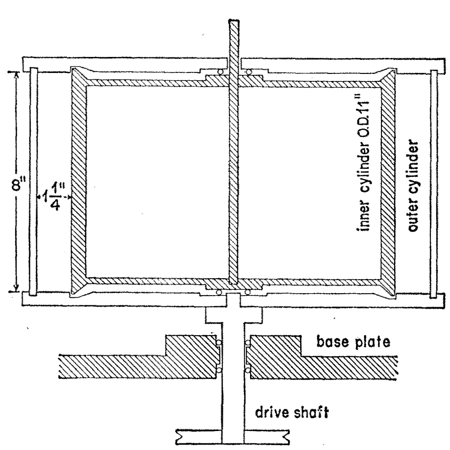

Fig. 1. Axial section of the apparatus. Hatched parts are held fixed.

Marker particles were made from candle wax and titanium dioxide powder by spraying a melted mixture. The solidified droplets were brilliant white spheres. Particles with the proper density were separated from sieved batches by flotation. The particle size best for film and lighting conditions was 0.15 mm. The outer cylinder was covered to leave exposed only a 4-mm band at midheight, and the light source, a Strobotac electronic stroboscope, illuminated a horizontal tabular volume of the flow. To ensure steady-state flow, the apparatus, filled with distilled water and suspended marker particles, was run for 10 minutes before pictures were taken.

A Polaroid camera was mounted pointing vertically upward into the flow. Two factors governed exposure: (i) total exposure time was limited by background fogging to about 2 seconds; (ii) it was desirable to limit the number of trajectories photographed at the same time, because these tend to be correlated. Each photograph was exposed about ten times for a few tenths of a second at intervals of a few seconds, with a particle concentration such that usually only one or two trajectories were obtained during each exposure; five to ten substantially independent trajectories were thus obtained on each photograph (Fig. 2).

The measuring arrangement consisted of a stationary binocular microscope over a horizontal stage that traveled in two perpendicular directions by means of threaded shafts. By suitably aligning a photograph on the stage, the coordinates of each image along a trajectory could be measured, by dials on the shafts, in a Cartesian x, y coordinate system formed by lines inscribed through the center and parallel to the sides of the photograph (Fig. 2). For each trajectory the quantities $\Delta x = x_{i+1} - x_i$ and $\Delta y = y_{i+1} - y_i$, the differences in x and y coordinates between successive points, were plotted versus point number i along the trajectory (Fig. 3). Smoothing of the scatter is important, because velocities used in momentum flux computations are based on measured coordinate differences, and velocities from unsmoothed differences fluctuate strongly. As the scatter seemed not to be inherent in the particle motion, smooth curves were drawn by hand to the plots of Δx_i and Δy_i versus i and the ordinates of the curves at the abscissae i were substituted for the measured differences.

There are three possible causes for the scatter. (i) It could be inherent in the particle motions. If the minimum scale of the turbulence was smaller than distances traveled by particles between flashes, intermediate points would be needed to draw curves representing true particle motions. (ii) It could be caused by imperfection in film or optics. Centers of images would not represent centers of particles. (iii) It could be caused by error in measuring centers of particles. The third possibility is excluded because the coordinates of well-defined points are closely reproducible. However, the coarse grain structure of the extremely fast film causes images of poorly illuminated or poorly focused particles to be indistinct. Two lines of evidence indicate that this, rather than the nature of the particle motions, causes the scatter. First, considering that diffuse, irregular images are as large as 0.3 mm, uncertainty in locating the points representing centers of particles can easily account for the maximum scatter of about 0.2 mm in Δx_i and Δy_i; second, there is a direct relation between sharpness of images along a trajectory and goodness of fit when a smooth curve is drawn through the measured coordinate differences (Fig. 4).

The velocities easiest to obtain from the trajectory data are tangential and radial velocity components u_i and v_i averaged between successive image points i and $i + 1$,

$$u_i = [(\theta_{i+1} - \theta_i)(r_{i+1} + r_i)/2]/\Delta t$$
$$v_i = (r_{i+1} - r_i)/\Delta t$$

where r_i and θ_i are the coordinates of the ith point on the trajectory with respect to a polar coordinate system centered on the axis of the cylinders and with radii in the illuminated plane, and Δt is the flash interval, 2.4×10^{-3} second. These closely approximate true particle velocities at points on the trajectory midway between the measured points if distances between points are small compared to radii of curvature along the trajectory, as is mostly the case. The u_i, v_i were associated with points whose polar coordinates are the averages of the polar coordinates of the two successive points (this leads to some deviation from true trajectory midpoints where radii of curvature are smallest). All velocity computations, after smoothing of coordinate differences, were done on an IBM 7094 computer; for each trajectory, the x_i, y_i were built from the smoothed differences Δx_i, Δy_i, the r_i, θ_i were obtained by transforming to a polar system, and the u_i, v_i were computed.

Velocities used in computing momentum flux were derived from the u_i, v_i by interpolating to obtain velocity components U, V associated with preassigned radii R_j in the flow. During computations for each trajectory, an interpolation was made whenever the radial coordinates of trajectory midpoints straddled one of the R_j:

$$U = u_{i-1} + [(u_i - u_{i-1})(R_j - r_{i-1})/(r_i - r_{i-1})]$$
$$V = v_{i-1} + [(v_i - v_{i-1})(R_j - r_{i-1})/(r_i - r_{i-1})]$$

where U and V are the tangential and radial velocity components, respectively, formed by interpolating between the $(i-1)$th and ith positions along a trajectory. Radii were chosen at $r =$ 13.95 cm, near the inner boundary, and at intervals of 0.05 cm outward.

A curve of $\bar{u}$, the average tangential velocity, versus r was constructed by fitting a smooth curve to a plot versus r of the average of all the velocities U at each R_j (Fig. 5). Fluctuating tangential velocities U' at any R_j can then be found from the relation $U' = U - \bar{u}$. Fluctuating radial velocity V' was assumed to be simply V, because secondary flow due to end friction should be small compared to turbulent fluctuations in the zone of strongest turbulence near the inner boundary. A grand average of all V values was found to be near zero, indicating that this assumption is valid.

Flux of tangential momentum in the radial direction, $-\rho\overline{u'v'}$, was computed for the inner third of the annulus by finding $U'V'$ for each interpolation at a given R_j and taking the average of these products over all N interpolations at that R_j,

$$\left[\sum_{i=1}^{N} (U'V')_i\right] /N$$

The density was taken to be 1 g/cm^3. Though the momentum flux values lie mostly between 5 and 20 dyne/cm^2, they show considerable scatter (Fig. 6); this is to be expected, because only 10 to 20 pairs of fluctuating velocities were used in forming each value (*6*). However, taken as a whole the momentum flux values involve well over a hundred trajectories, so that a grand aver-

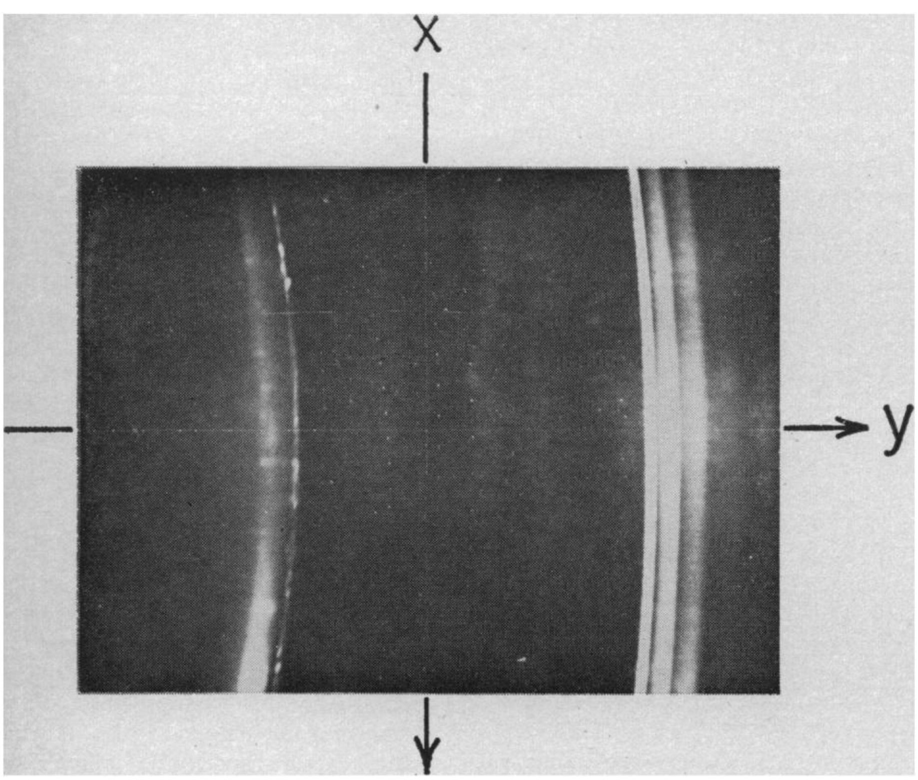

Fig. 2. A typical photograph. The two bands of light nearest the center represent intersections of the light beam with the flow boundaries; the other bands are reflections. Particle trajectories show up as sequences of illuminated dots.

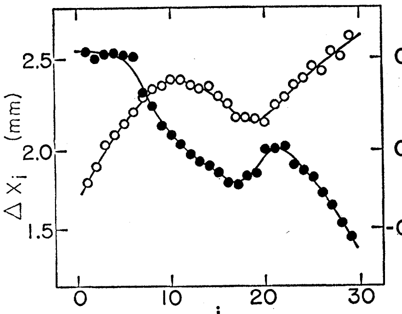

Fig. 3. Coordinate differences Δx_i and Δy_i versus image number i for a representative trajectory near the inner boundary.

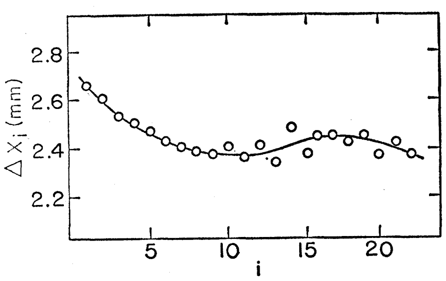

Fig. 4. Δx_i versus image number i for a trajectory whose images become less distinct from left to right; there is a corresponding increase in the scatter.

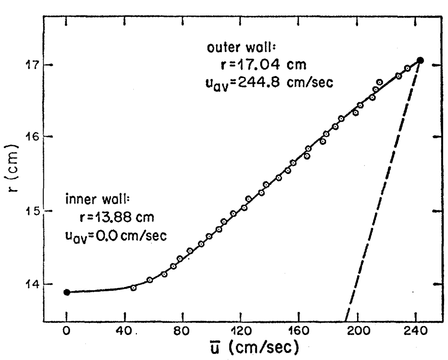

Fig. 5. Average tangential velocity versus radius. The open circles represent the known velocities of the inner and outer boundaries. The dashed line shows rigid-body velocities of the end plates.

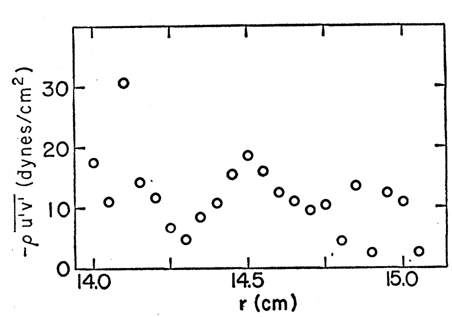

Fig. 6. Computed momentum flux versus radius.

age of the momentum flux values (12 to 13 dyne/cm^2) representing the entire zone should be close to momentum flux values based on a much larger number of trajectories.

Ideally, the computed momentum flux should be checked by adding the shear stress due to mean motion, to obtain the total shear stress, and then evaluating the total shear stress independently by measuring torque on the inner cylinder. There is no straightforward way of doing this, because secondary flow due to end friction causes the distribution of total shear stress across the annulus to vary with distance from the ends. A satisfactory check can nonetheless be made by determining the total shear stress at the inner boundary from the slope of the mean velocity curve there and assuming that the total shear stress does not decrease greatly from the inner wall to the zone where the momentum flux was computed.

The shear stress due to mean motion in the zone where momentum flux was computed was found by measuring the velocity gradient, about 100 cm sec^{-1} sec^{-1}, from Fig. 5 in the range 14.00 to 14.50 cm and using the relation $\tau = \mu(d\bar{u}/dr)$. The result, 1 dyne/cm^2, is so small that the measured momentum flux represents quite closely the total shear stress. Very near the inner boundary, where the turbulent momentum flux decreases to zero and the shear stress is due entirely to laminar flow, the mean velocity gradient increases very sharply. The slope of the $\bar{u}$ versus r curve at the inner wall can be estimated reliably, because the position of the inner wall was measured at the same time as the coordinates of the images. The total shear stress in the immediate vicinity of the inner wall determined in this way is 25 ± 5 dyne/cm^2. The total shear stress in the zone where momentum flux was computed is thus smaller than the total shear stress at the inner wall by no more than a factor of 2, so that the computed momentum flux should be less than the true momentum flux by no more than a factor of 2. Actually, the agreement may be much closer, depending upon how rapidly the true total shear stress decreases away from the inner wall.

Thus, the foregoing method of measuring momentum flux should suffice to obtain a value for the momentum transport ratio that is in error by considerably less than a factor of 2, because the momentum transport ratio defined above involves the quotient of two values of momentum flux which, owing to the experimental method, should differ from the respective true values by about the same factor. The method is thus certainly sensitive enough to provide a test of Bagnold's grain-collision theory.

J. B. SOUTHARD

Division of Geological Sciences, California Institute of Technology, Pasadena 91109

References and Notes

1. R. A. Bagnold, *Proc. Roy. Soc. London Ser. A* **225**, 49 (1954).
2. ———, *Phil. Trans. Roy. Soc. London Ser. A* **249**, 235–297 (1956); *U.S. Geol. Surv. Profess. Papers No. 422-I* (1966).
3. H. Schlichting, *Nachr. Akad. Wiss. Goettingen II Math.-Physik. Kl.*, 160–197 (1932).
4. F. Schultz-Grunow, *Z. Angew. Math. Mech.* **39**, 101 (1959).
5. H. Schlichting, *Boundary Layer Theory* (McGraw-Hill, New York, 1960), p. 430.
6. V. A. Vanoni and N. H. Brooks, *California Institute of Technology Hydrodynamics Laboratory Report E-46* (1955).

7. Supported by NSF graduate fellowship funds and by the Committee on Experimental Geology and Geophysics at Harvard University. I thank A. V. Jopling and R. Siever for their advice and encouragement.

17 April 1967

Seed from the Upper Devonian

Abstract. *We present evidence proving the existence of seeds in the Upper Devonian and extending the known age of seed plants from the Lower Carboniferous (Mississippian) into the Upper Devonian.*

The origin of seed plants is one of the most interesting problems in the fossil history of the vascular plants. In the Lower Devonian, vascular plants were entirely homosporous. The late Devonian saw attainment of heterospory in some lycopsids and some macrophyllous plants, and hitherto it is from the Lower Carboniferous (Mississippian) that fossils that are unquestionably seeds are first recorded.

Recent discovery (*1*) of megaspore tetrads (*Cystosporites devonicus*) in the Upper Devonian, in which a single, large, presumably functional megaspore was developed at the expense of the other three members of the tetrad, demonstrates that by the late Devonian one group of plants had attained a markedly high level of heterospory. More recently (*2*) it has been shown that this type of tetrad organization occurs in some authenticated Lower Carbonifer-